Impact of Surface Waves on Wind Stress under Low to Moderate Wind Conditions

SHENG CHEN

First Institute of Oceanography, Ministry of Natural Resources, and Laboratory for Regional Oceanography and Numerical Modeling, Qingdao National Laboratory for Marine Science and Technology, Qingdao, China

FANGLI QIAO

First Institute of Oceanography, Ministry of Natural Resources, and Laboratory for Regional Oceanography and Numerical Modeling, Qingdao National Laboratory for Marine Science and Technology, and Key Laboratory of Marine Sciences and Numerical Modeling, Ministry of Natural Resources, Qingdao, China

WENZHENG JIANG, JINGSONG GUO, AND DEJUN DAI

First Institute of Oceanography, Ministry of Natural Resources, and Laboratory for Regional Oceanography and Numerical Modeling, Qingdao National Laboratory for Marine Science and Technology, Qingdao, China

(Manuscript received 3 January 2019, in final form 20 May 2019)

ABSTRACT

The impact of ocean surface waves on wind stress at the air–sea interface under low to moderate wind conditions was systematically investigated based on a simple constant flux model and flux measurements obtained from two coastal towers in the East China Sea and South China Sea. It is first revealed that the swell-induced perturbations can reach a height of nearly 30 m above the mean sea surface, and these perturbations disturb the overlying airflow under low wind and strong swell conditions. The wind profiles severely depart from the classical logarithmic profiles, and the deviations increase with the peak wave phase speeds. At wind speeds of less than 4 m s^{-1}, an upward momentum transfer from the wave to the atmosphere is predicted, which is consistent with previous studies. A comparison between the observations and model indicates that the wind stress calculated by the model is largely consistent with the observational wind stress when considering the effects of surface waves, which provides a solution for accurately calculating wind stress in ocean and climate models. Furthermore, the surface waves at the air–sea interface invalidate the traditional Monin–Obukhov similarity theory (MOST), and this invalidity decreases as observational height increases.

1. Introduction

Wind stress over the ocean is a key parameter for understanding the physical processes in both the atmosphere and ocean. Determination of the wind stress is important for coupled ocean–atmosphere modeling, weather forecasting and other applications. The ocean surface is mobile in contrast with rigid land, and surface waves play a significant role in the boundary layer dynamics between the upper ocean and lower atmosphere (Grachev and Fairall 2001; Veron et al. 2009; Babanin et al. 2012). The influence of surface waves on wind stress has been widely recognized through field observations (Donelan et al. 1997; Grachev et al. 2003; Högström et al. 2015), laboratory experiments (Uz et al. 2003; Makin et al. 2007; Buckley and Veron 2018), and numerical models (Janssen 1989; Makin 2008; Jiang et al. 2016; Babanin et al. 2018).

In the presence of surface waves, the total velocity can be separated into three parts: mean, turbulent, and wave-induced components of airflow (Hare et al. 1997). In this situation, the total stress τ_{tot} above the surface waves can be expressed as follows:

$$\tau_{tot} = \tau_{turb} + \tau_{wave} + \tau_{visc}. \quad (1)$$

Denotes content that is immediately available upon publication as open access.

Corresponding author: F. Qiao, qiaofl@fio.org.cn

DOI: 10.1175/JPO-D-18-0266.1

Here τ_{turb} is the turbulent shear stress, τ_{wave} is the wave-induced stress, and τ_{visc} is the viscous stress that is assumed to be negligible (Hanley and Belcher 2008). The total wind stress can be represented by $\tau_{tot} = C_D U^2$ according to the bulk formula, C_D is the drag coefficient, and U is the wind speed. Within a layer not affected by waves, the wave-induced stress equals zero, and the total stress equals the turbulent stress. The wave-induced stress is strongly dependent on the wave age (Hanley and Belcher 2008). For young wind seas, the wave extracts momentum from the wind so that the wave-induced stress is positive ($\tau_{wave} > 0$; Komen 1994) and the momentum flux is always directed downward (Semedo et al. 2009); with increasing wave age, τ_{wave} decreases until reaching zero, and the sign is reversed for old seas, and becomes negative ($\tau_{wave} < 0$; Smedman et al. 1999; Grachev and Fairall 2001). In the situation of $\tau_{wave} < 0$ and $|\tau_{wave}| > |\tau_{turb}|$, the total stress becomes negative ($\tau_{tot} < 0$), meaning that upward momentum transfer from the ocean to the atmosphere.

Mixed wind sea and swell or pure swell conditions are the most common in the ocean. Wind seas are generated locally and travel more slowly; in contrast, swells are usually generated remotely and travel faster than the local wind (Hanley and Belcher 2008). Janssen (1989) found a considerable enhancement of momentum transfer for young wind seas according to a quasi-linear wind-wave model. In a subsequent study, he proposed that the stress over the surface wave is dependent on the wind speed and wave-induced stress (Janssen 1992). There is some evidence from field observations and numerical simulations to support that the swell can lead to dramatic changes in wind stress and modulate the wind profiles (Semedo et al. 2009; Song et al. 2015; Jiang et al. 2016; Zou et al. 2018). Under low wind conditions, the faster-traveling swell could result in an upward momentum transfer ($\tau_{tot} < 0$) from the ocean to the atmosphere, which has a considerable effect on the turbulence structure of the whole marine atmospheric boundary layer (Drennan et al. 1999; Grachev and Fairall 2001; Semedo et al. 2009; Nilsson et al. 2012). In addition, swell-induced perturbations have been observed at heights greater than 10 m, causing distinct peaks at the dominant swell frequency of the turbulent velocity spectra (Rieder and Smith 1998; Högström et al. 2015; Chen et al. 2018), and the vertical velocity is more coherent with the swells than the horizontal velocity (Grare et al. 2013).

While the aforementioned studies have provided new insights into these complicated phenomena, the water depth factor is not considered in numerical models (Hanley and Belcher 2008; Semedo et al. 2009; Zou et al. 2018). Surface waves in the coastal regions with finite depth behave differently than surface waves in the open ocean (Huang et al. 1983). Additionally, wind stress depends on the surface wave states, which are affected by depth-induced processes in shallow water areas (Zhao et al. 2015). In the present study, we investigate the influence of surface waves on wind stress under different sea states and water depth conditions using numerical models and field observations over northern South China Sea (SCS) and western East China Sea (ECS) coastal regions.

This study is organized as follows. The field observations from two coastal regions and the datasets used in the comparisons are described in section 2. A simple constant flux model that includes wave-induced stress parameterizations is presented in section 3. The water depth factor is considered in the model to indicate the impact of surface waves on the wind stress, and the results of comparisons with observations are also described in this section. Finally, our conclusions are summarized and discussed in section 4.

2. Field observations

The two finite-depth field measurements used in this study were obtained from the BoHe observation tower (BHOT) in the northern SCS and from the DongOu observation tower (DOOT) in the western ECS (Fig. 1). The tower is more suitable for flux measurements and provides less flow distortion and motion influence than a conventional shipborne system. An eddy covariance system was mounted 17 m above the mean sea surface and 6 m away from the bulky platform, toward 70° north by east. This eddy covariance system was used to observe the momentum and heat fluxes, and a bottom-supported acoustic wave and current (AWAC) buoy was deployed at a mean water depth of approximately 16 m (Fig. 1b) to record the surface displacement at the BoHe site (21°26.5′N, 111°23.5′E). Details of this setup can be found in Chen et al. (2018).

The DOOT is located at 27°40′N, 121°21′E, which is approximately 24 km from the coastline (Fig. 1a). The mean water depth at this site is approximately 28 m. The site has a 7-m tower at the platform, which has a hollow structural steel frame. To avoid the flow distortion caused by the bulky platform, eddy covariance system probes, including a three-dimensional ultrasonic and infrared gas analyzer, were mounted at the northeast corner of the tower, approximately 26 m above the mean sea surface, toward 30° north by east and were fixed to a stable boom that extended vertically upward 2 m from the tower top and horizontally outward approximately 0.5 m (Fig. 1c). During the observational periods, an AWAC buoy was also deployed on the

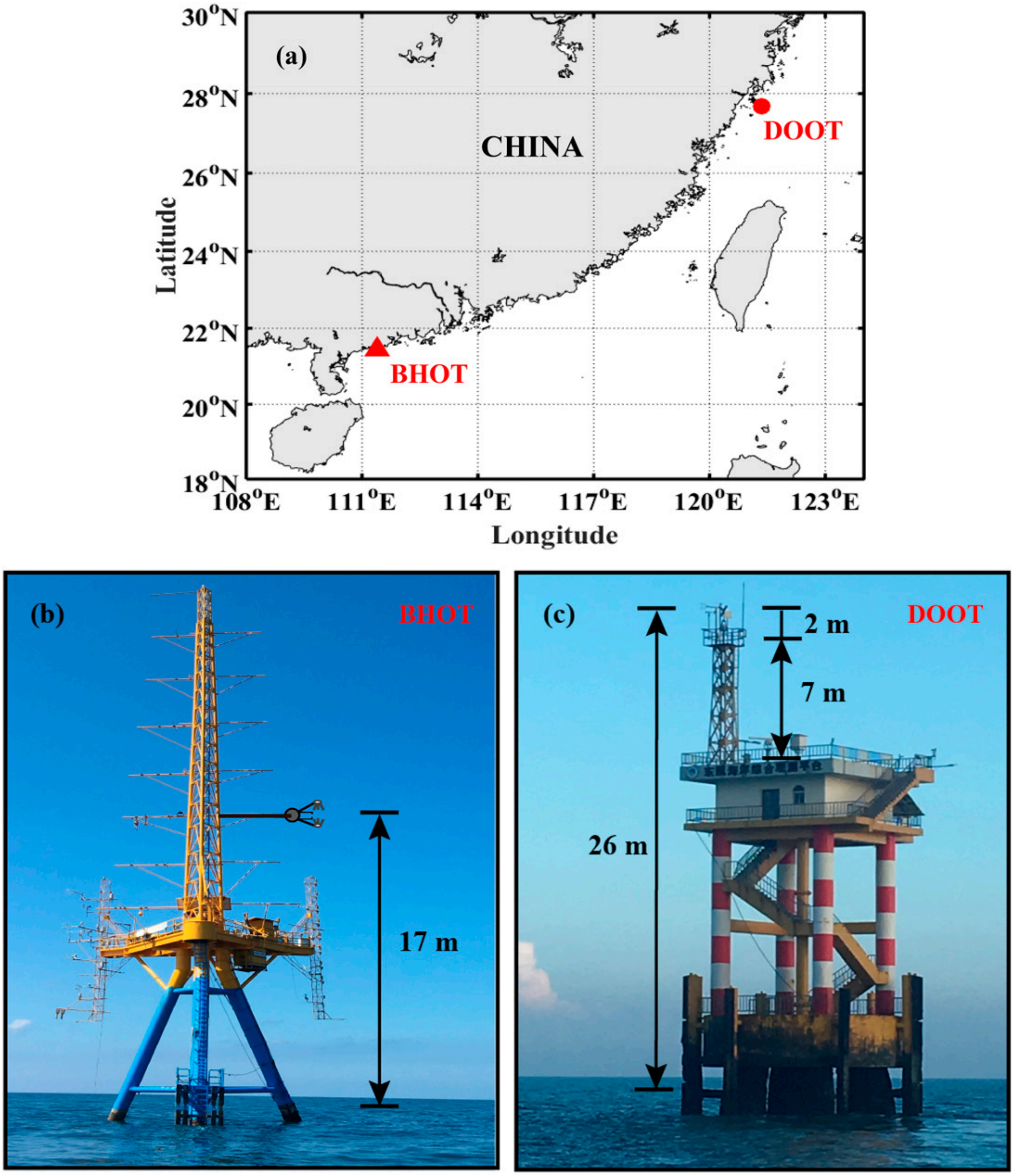

FIG. 1. (a) Regional map and locations of the BHOT and DOOT and photos of the (b) BHOT and (c) DOOT.

seabed to simultaneously measure surface waves near this tower site.

a. Basic information

The momentum flux and surface wave datasets with average time intervals of 1 h from 10 February to 11 March 2015 for the BHOT and from 1 to 30 April 2017 for the DOOT were selected and analyzed in this study. Due to a variety of unfavorable factors, such as rain and unstable voltage, some of the measurement data are missing; therefore, 694 and 519 measurements were obtained at the BHOT and DOOT sites, respectively. In addition, the swell significant wave height H_s^{swell} and wind sea significant wave height H_s^{windsea} were calculated based on the one-dimensional wave spectrum (Högström et al. 2015).

The entire time series of the two observational sites for wind speed, significant wave height including H_s^{swell} and H_s^{windsea}, and drag coefficient C_D are shown in Figs. 2 and 3. During the BHOT observational periods, the winds were not strong, with a maximum of nearly 13 m s^{-1}, and with an average of approximately 6 m s^{-1} (Fig. 2a). The significant wave height varied between 0.4 and 2.4 m, and swells prevailed over the wind seas under

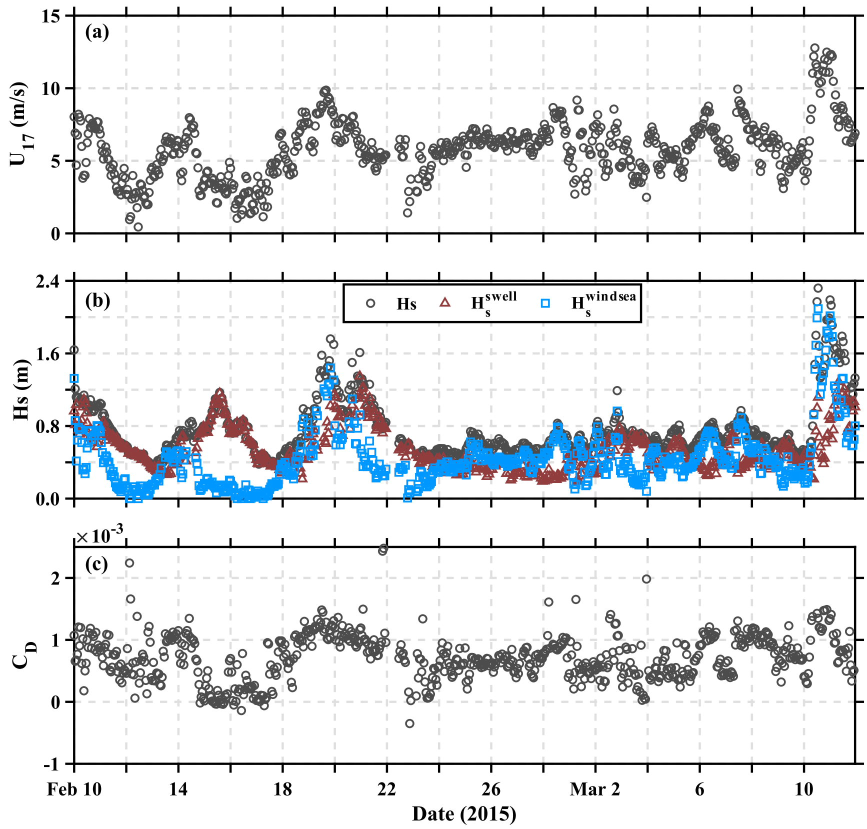

FIG. 2. Time series of (a) wind speed U; (b) significant wave height H_s (dark gray circle), swell H_s^{swell} (brown triangle), and wind sea H_s^{windsea} (blue square) significant wave heights; and (c) drag coefficient C_D at the BHOT site. Wind speed and flux were observed at a height of approximately 17 m.

wind conditions with wind speeds of less than 6 m s^{-1}, which accounted for more than 50% of the wind conditions. When the wind speed exceeded 6 m s^{-1}, the wind sea height increased and exceeded the swell height (Fig. 2b). The drag coefficients C_D values were related to the winds, and under low wind conditions, some values (12 cases) were below zero (Fig. 2c), which indicates an upward momentum transfer from the ocean to the atmosphere.

The conditions during the DOOT observational periods were variable, with wind speeds from 0 to 13 m s^{-1}, and the mean wind speeds was nearly 5 m s^{-1} (Fig. 3a). The significant wave height ranged from 0.4 to 2.0 m, and similar to the BHOT periods, swells were dominant under low wind conditions that exceeded 80% of the total, and the wind seas began to increase as the wind speed increased (Fig. 3b). The drag coefficient C_D values were below zero in 31 measured cases under low wind conditions (Fig. 3c). Notably, the wind stress in this study includes only the along-wind stress component $-u'w'$, which was used for comparison with the model; correspondingly, the drag coefficient includes only the along-wind component. Additionally, nonstationary motions were removed before wind stress calculations to better illustrate the effects of surface waves on the stress (Chen et al. 2018).

b. Swell effect on velocity spectra

To indicate the swell effect on the observed velocity and clarify the differences in this effect for different observational heights, the velocity spectra were considered in this section. Grare et al. (2013) showed that the vertical airflow velocity is more significantly influenced by the waves with respect to the horizontal velocity. Therefore, all the vertical velocity w spectra with distinct spectral peaks and 1D wave spectra are shown in Fig. 4 for the BHOT and DOOT observational periods, including the overall mean spectrum. Distinct peaks of approximately 0.115 Hz at the dominant swell frequency were observed in 66 and 53 measurements during the BHOT and DOOT observational periods, respectively, with wind speeds of less than 6 m s^{-1}, accounting for approximately 10% of the total. This finding indicated that the waves modulated the airflow and induced a

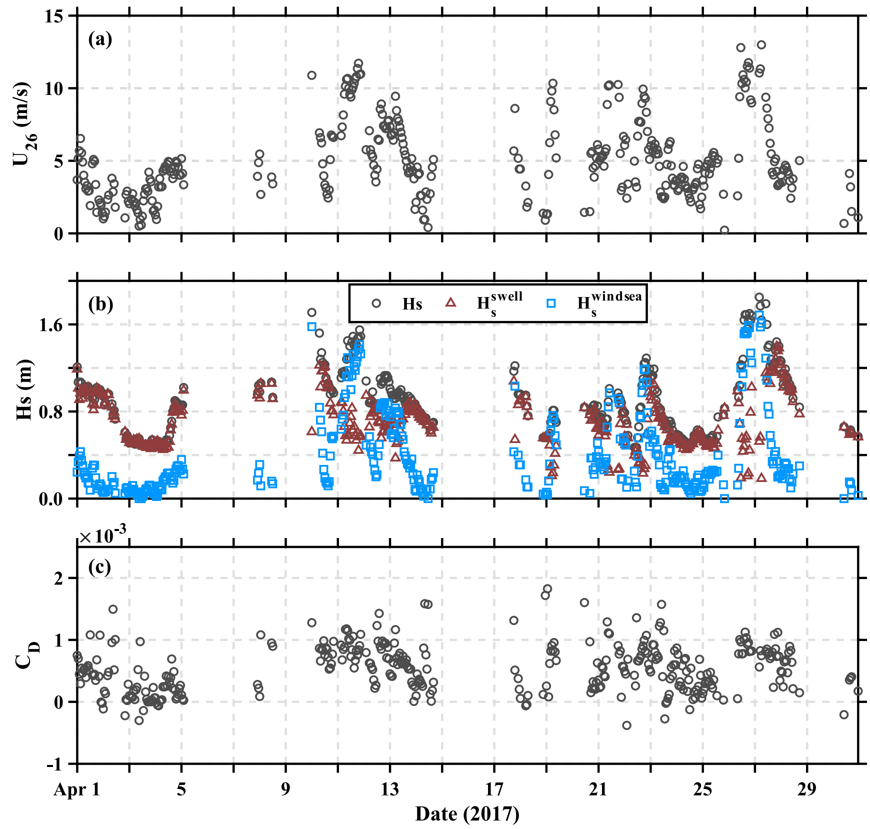

FIG. 3. As in Fig. 2, but for the DOOT site. Wind speed and flux were observed at a height of approximately 26 m.

velocity fluctuation which was phase locked with the waves (Hristov et al. 1998). Consequently, the observed velocity is the sum of the turbulent and wave-induced velocities; however, decomposition is extremely difficult (Hristov et al. 1998).

The wave spectra showed nearly the same peak frequencies during both observational periods. In addition, the mean wind speeds for all these measurements with prominent spectral peaks were approximately $3\,\mathrm{m\,s^{-1}}$ at the BHOT and $2.5\,\mathrm{m\,s^{-1}}$ at the DOOT, but the mean vertical velocity spectral peak at the DOOT was less than that at the BHOT (Figs. 4a,b). The measurement height was approximately 26 m above the mean sea surface at the DOOT, which was higher than approximately 17 m at the BHOT. This finding meant that the peak amplitudes decreased with increasing height, similar to the results based on four levels of observations (~5, 7, 10, and 14 m) reported by Högström et al. (2015). Hristov et al. (2003) stated that the wave-induced velocity decayed exponentially with height; thus, the velocity spectral peaks at the dominant swell frequency decreased with increasing observational height under nearly the same wave conditions.

The swell-induced perturbations reached 26 m above the mean sea surface, which meant that the wave-induced stress component was incorporated into the total stress. Consequently, a simple model considering the wave-induced stress is applied to evaluate the influence of surface wave on the total wind stress in the following section.

3. Modeling

Based on the assumptions of a negligible Coriolis term and stationary flow with no horizontal pressure gradients, and total stress and its turbulent and wave-induced components along the wind direction (Semedo et al. 2009), the constant flux model was used in this study to analyze the impact of surface waves on the wind stress. The momentum conservation equation can be simplified as follows:

$$\frac{d\tau_{\mathrm{tot}}}{dz} = 0. \qquad (2)$$

Here, z is the vertical coordinate, and τ_{tot} is defined as $-u'w'$, where u' and w' are the horizontal and vertical

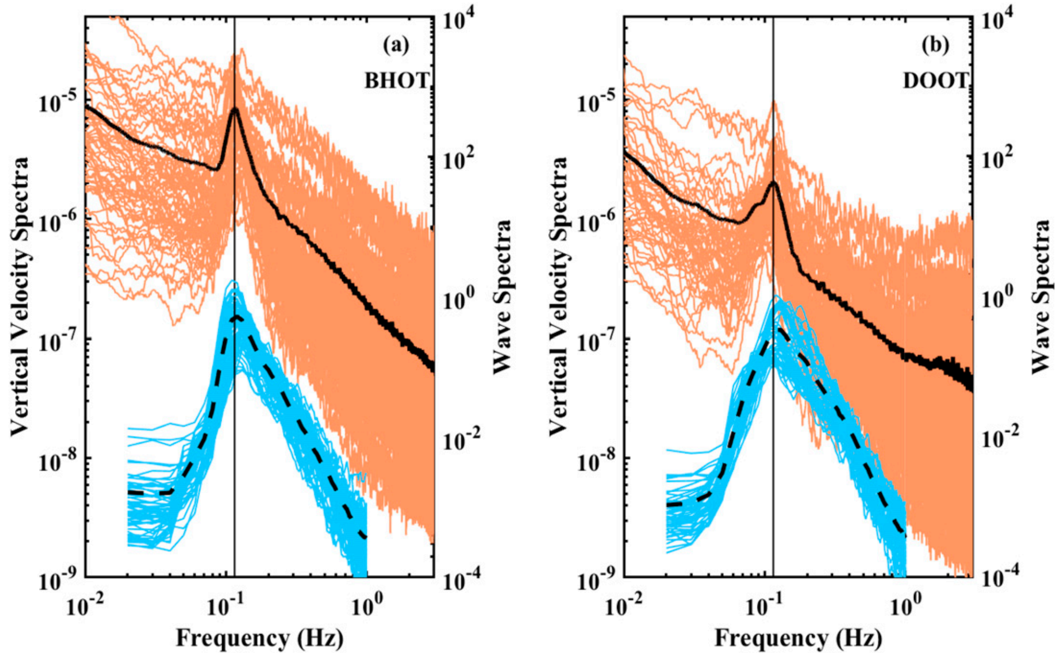

FIG. 4. All vertical velocity w spectra with distinct spectral peaks (red lines) and wave spectra (blue lines) plotted against frequency for the (a) BHOT (66 measurements) and (b) DOOT (53 measurements) sites; the solid and dashed lines represent the mean w and wave spectra, respectively. The vertical thin black lines represent the peak frequency ($f_p = 0.115$ Hz) of the mean w spectra.

velocity fluctuations, respectively. Although Eq. (2) has been accepted and appeared in previous publications, it should be noted that the stationary flow with no horizontal pressure gradients is an assumption, which means that if the balanced horizontal pressure gradient is needed remains an open question. Additionally, the constant flux layer assumption may be debatable due to the momentum flux divergence (Smedman et al. 2009; Mahrt et al. 2018), but some basic physical processes, such as the surface wave effect on wind stress, can be illustrated through it (Semedo et al. 2009; Babanin et al. 2018; Zou et al. 2018); therefore, the constant flux layer assumption is adopted in this study.

When $\tau_{\rm visc}$ is omitted, Eq. (1) becomes the following equation:

$$\tau_{\rm tot} = \tau_{\rm turb} + \tau_{\rm wave} = u_*^2 . \tag{3}$$

Here, $u_* = \sqrt{\tau_{\rm tot}}$ is the friction velocity, and note that when the total stress becomes negative, $u_* = \sqrt{(|\tau_{\rm tot}|)}$. The turbulent stress $\tau_{\rm turb}$ can be parameterized as follows:

$$\tau_{\rm turb} = K_m \frac{dU}{dz}. \tag{4}$$

Here, U is the mean horizontal wind speed, and by combining Eqs. (3) and (4), the wind profile above the surface wave can be expressed as follows:

$$U(z) = \int_{z_0}^{z} (\tau_{\rm tot} - \tau_{\rm wave}) K_m^{-1}\, dz . \tag{5}$$

Here, z_0 is the viscous roughness length (Zou et al. 2018), and K_m is the turbulent eddy viscosity. According to the Monin–Obukhov similarity theory (MOST), under neutral conditions, K_m can be obtained by the following equation:

$$K_m = l u_* . \tag{6}$$

This equation is denoted as the MOST model, and the wave effect is not considered in the MOST model, which means $\tau_{\rm wave} = 0$ in Eq. (5). Here, $l = \kappa z$ is the mixing length, and $\kappa = 0.4$ is the von Kármán constant. However, by considering the surface wave effect and following Semedo et al. (2009), the eddy viscosity, which is based on the turbulent kinetic energy (TKE) equation, can be expressed as follows:

$$K_m^4 l^{-4} = |\tau_{\rm tot}(\tau_{\rm tot} - \tau_{\rm wave}) + K_m F_w| . \tag{7}$$

This equation denotes the S09 model, and F_w is the wave-induced pressure perturbation term. Variables $\tau_{\rm wave}$ and F_w can be parameterized in accordance with Semedo et al. (2009):

$$\tau_{\text{wave}} = \int_0^\infty \frac{\beta \rho_w g S(f)}{\rho_a c} e^{-2kz}\, df, \quad \text{and} \tag{8}$$

$$F_w = -2kc\tau_{\text{wave}}. \tag{9}$$

Here, ρ_w, and ρ_a are the water and air densities, respectively; g is the acceleration of gravity; $S(f)$ is the wave frequency spectrum; f is the frequency; c is the wave phase speed; k is the wavenumber; and β is the wave growth/decay rate, which can be written as follows (Belcher and Hunt 1993):

$$\beta = C_\beta k \frac{\rho_a}{\rho_w}\frac{u_*^2}{c}. \tag{10}$$

Here, C_β is the wave growth/decay rate coefficient. By combining the wave tank experiment and field observations, Plant (1982) concluded that C_β had a value of approximately 32 ± 16 for a wave age of $c/u_* < 20$.Conversely, Cohen and Belcher (1999) showed that C_β was negative ($C_\beta \approx -10$) for fast waves ($c/u_* > 20$), and Hanley and Belcher (2008) used a relatively large value of $C_\beta = -30$.

Following Hanley and Belcher (2008), the wind-wave frequency spectrum is calculated by the formula suggested by Donelan et al. (1985):

$$S(f) = \frac{\alpha g^2 f^{-4}}{(2\pi)^4} f_p^{-1} \exp\left[-\left(\frac{f_p}{f}\right)^4\right]\gamma^\Gamma. \tag{11}$$

Here, $\Gamma = \exp[-(f-f_p)^2/(2\sigma^2 f_p^2)]$. According to Donelan et al. (1985), $\alpha = 0.006(U_{10}/C_p)^{0.55}$, $\sigma = 0.08[1 + 4/(U_{10}/C_p)^3]$, and $\gamma = 1.7 + 6.0\log(U_{10}/C_p)$ is the peak enhancement factor, where f_p is the frequency at the spectrum peak, C_p is the corresponding wave phase speed, and U_{10} is the 10-m wind speed. Huang et al. (1983) indicated that the wave spectrum was affected by the water depth and proposed the Wallops spectrum based on Stokes waves in finite water depth [$1 < kh < 3$; here, h is the water depth, and the dispersion relation is $(2\pi f)^2 = gk\tanh(kh)$]:

$$S(f) = \frac{\alpha_f g^2}{(2\pi)^4 f_p^5}\left(\frac{f_p}{f}\right)^m \exp\left[-\frac{m}{4}\left(\frac{f_p}{f}\right)^4\right]. \tag{12}$$

Here, $\alpha_f = \alpha_d \tanh^2(k_p h)$ is the finite water depth coefficient, α_d is for deep water waves, and m is the slope of the high-frequency side of the spectrum.

For deep water, $m = 5$ is suggested, but this value decreases with decreasing water depth (Huang et al. 1983). When the value equals 4, Eq. (11) is consistent with Eq. (12) without considering peak enhancement. Therefore, we adopt Eq. (11) to show the behavior of the model following Hanley and Belcher (2008); however, the coefficient α is modified and multiplied by the water depth factor $\tanh^2(k_p h)$. The wind waves are generated by the local wind, and the swells are remotely generated by high winds so that the wave spectrum is the sum of the wind-wave and swell spectrum. Based on the wind-wave spectrum generated by a high wind speed, the swell spectrum is represented by the following equation (Hanley and Belcher 2008):

$$S(f) = S(f)\exp\left[\left(\frac{f}{f_0}\right)^3\right]. \tag{13}$$

Here, f_0 is the damping parameter, and $(2\pi f_0)^{-3} = -0.01$ is used in this study (Hanley and Belcher 2008).

a. *Behavior of the model*

Following Hanley and Belcher (2008), the wave growth/decay rate coefficient is distinguished by a wave age of $c/u_* = 20$, $C_\beta = 32$ is assigned for the wind-wave ($c/u_* < 20$), and $C_\beta = -30$ is assigned for the swell ($c/u_* > 20$); and all these values are used to qualitatively describe the behavior of the model under low wind and swell conditions. After the definitions of the growth/decay rate and wave frequency spectrum were obtained, the wave-induced stress was calculated using Eqs. (8), (11), and (13), and the solution to Eq. (5) was obtained. The model requires the following parameters to be assigned: the high wind speed that is used to calculate the swell spectrum, denoted as U_h, the local wind speed U_{10}, the water depth h, and the frequency at the spectrum peak f_p.

As stated in Fig. 4, the frequency of the swell spectra peak was approximately 0.115 Hz during both observational periods, so $f_p = 0.115$ Hz was assigned under low wind conditions. Here, the low wind speed U_{10} ranged from 1 to 6 m s^{-1}. Following Hanley and Belcher (2008), a ratio $R = \tau_{\text{wave}}(0)/\tau_{\text{turb}}(0)$ was defined, here $\tau_{\text{wave}}(0)$ and $\tau_{\text{turb}}(0)$ were the wave-induced stress and turbulent stress at the sea surface, respectively. Because the frequency at the spectrum peak f_p was fixed to a constant value, the wavenumber at the spectrum peak k_p decreased with increasing water depth h based on the shallow water dispersion relation $(2\pi f_p)^2 = gk_p\tanh(k_p h)$; therefore, the peak wave phase speed C_p increased with water depth. The wind profiles derived from the MOST and S09 models for different water depths and the ratio R calculated for different high wind speeds and water depths are shown in Fig. 5. The impact of swells on the wind profiles was significant. Under light wind and swell conditions, the wind profiles departed from the traditional logarithmic profiles, and the deviation increased with the peak wave phase speed,

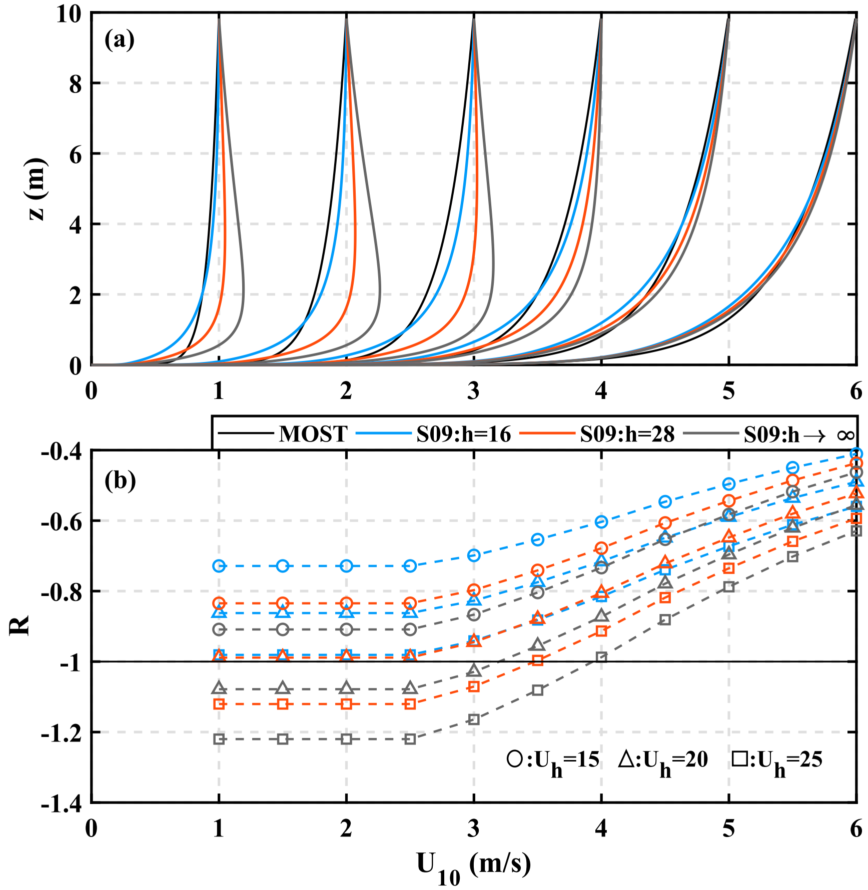

FIG. 5. (a) The wind profiles under high wind speed $U_h = 25\,\mathrm{m\,s^{-1}}$ condition and (b) the variation in R with wind speed U_{10} for different U_h values. The blue, red, and gray lines represent the wind profiles derived from the S09 model for shallow water depths of 16 and 28 m and deep water, respectively, and the thin black lines represent wind profiles derived from the traditional MOST in (a). The circles, triangles, and squares show $U_h = 15$, 20, and $25\,\mathrm{m\,s^{-1}}$, respectively, and the blue, red, and gray colors represent the shallow water depths of 16 and 28 m and deep water, respectively, in (b).

and the influence of swells decreased with increasing wind speed (Fig. 5a). Under lower wind and greater peak phase speed conditions, a wave-driven wind was predicted by the model, which was similar to the findings of Semedo et al. (2009) and Zou et al. (2018).

The necessary condition for a wave-driven wind was $R < -1$, which occurred when the high wind speeds and peak wave phase speeds were greater, and the local wind speeds were lower (Fig. 5b); these findings were consistent with the model results reported by Hanley and Belcher (2008). Under these swell-dominated conditions, the wave-induced stress was negative and induced an upward momentum transfer from the wave to the atmosphere, which was simulated by the S09 model that included the wave effect. Once the frequency at the spectrum peak f_p was fixed, deeper water induced a faster peak phase speed C_p. Faster waves with more energy provided a larger negative contribution to the wave-induced stress, as Hanley and Belcher (2008) discussed, and the negative stress magnitude increased with the peak wave phase speed C_p.

b. Comparison with the observations

The measurements obtained at the BHOT and DOOT sites were compared with the model. Before this comparison was completed, the wind stress and wave spectra underwent selection control based on the wind direction relative to the instrument orientation. If the winds originated from the probe rear, the flux data obtained by the system were of poor quality (Foken et al. 2012). Therefore, the datasets with a wind incident angle in the range of ±60° relative to the instrument rear were not included in this comparison, and, 683 and 359 measurements remained for the BHOT and DOOT sites,

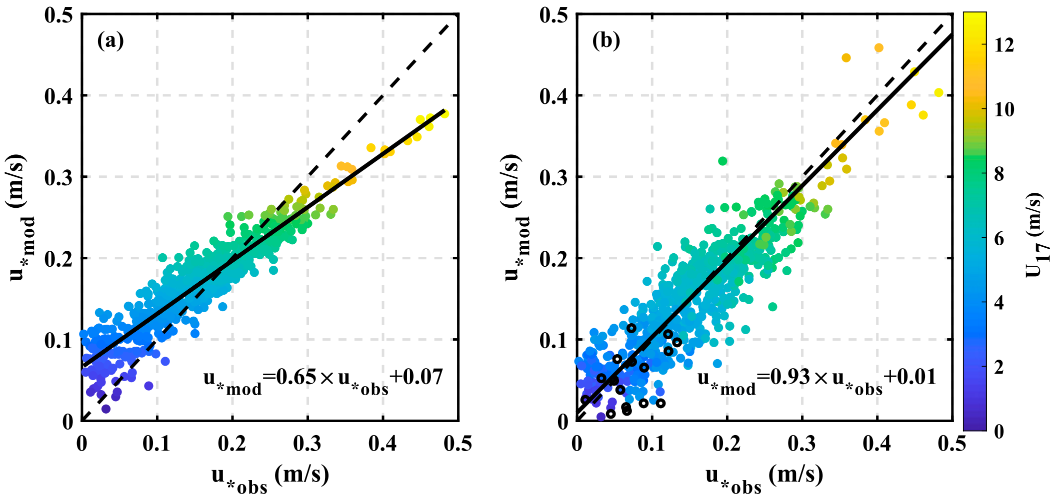

FIG. 6. Comparison between the modeled and observed friction velocities during the BHOT observational periods. (a) The traditional MOST model and (b) the S09 model that includes wave effects are used. The dashed and solid lines represent the 1:1 scale line and the fitted line between the modeled and observed results, respectively. The black circles represent the friction velocity values corresponding to the negative stress values of the model output.

respectively. The parameterization of the wave growth/decay rate coefficient C_β had remained uncertain until now (Hanley and Belcher 2008; Semedo et al. 2009; Zou et al. 2018). Hence, the wave growth rate coefficient was assigned a value of 16 as a result of the better fit with the observations under higher wind conditions, and with reference to Hanley and Belcher (2008), a value of −30 was used as the decay rate coefficient to assess the effect of the surface waves on wind stress in this section. The required parameters were input into the model, including the observed wind speed, observational height, water depth, and observed 1D wave spectra, which were divided into two parts based on the wave age of $c/u_* = 20$.

The comparisons of the observed wind stress and model (MOST and S09) results for both the BHOT and DOOT observational periods are shown in Figs. 6 and 7. The friction velocity calculated by the traditional MOST model deviated greatly from the observed values during the BHOT observational periods. The simulated friction velocity was greater than the observational friction velocity u_* below $0.2\,\mathrm{m\,s^{-1}}$, with a positive bias of $0.027\,\mathrm{m\,s^{-1}}$ and smaller for $u_* > 0.2\,\mathrm{m\,s^{-1}}$, with a negative bias of $-0.026\,\mathrm{m\,s^{-1}}$ (Fig. 6a). Notably, the friction velocity at $0.2\,\mathrm{m\,s^{-1}}$ corresponded to the wind speed at approximately $6\,\mathrm{m\,s^{-1}}$. However, by considering the surface wave effects, the friction velocity calculated by the S09 model showed good quantitative agreement with the observed values, and the bias was extremely small ($0.007\,\mathrm{m\,s^{-1}}$ for $u_* < 0.2\,\mathrm{m\,s^{-1}}$ and $-0.008\,\mathrm{m\,s^{-1}}$ for $u_* > 0.2\,\mathrm{m\,s^{-1}}$, Fig. 6b). Under low wind conditions, the swell dominated the wave field, which induced a swell-dominated spectrum and contributed to a negative wave-induced stress. As Jiang et al. (2016) concluded, the stress derived from the traditional MOST was greater than the actual total stress under swell conditions. In contrast, the wind waves gradually became dominant under the higher wind conditions, which produced a positive wave-induced stress. As Janssen (1992) discussed, for the wind seas, the wave-induced stress could result in a considerable enhancement of the wind stress, both of which led to the S09 model results better predicting the wind stress.

During the DOOT observational periods, the friction velocity calculated by the MOST model also deviated from the observed values (Fig. 7a), but after consideration of the wave effects, the biases changed from 0.026 to $0.002\,\mathrm{m\,s^{-1}}$ and from −0.014 to $-0.004\,\mathrm{m\,s^{-1}}$ for friction velocities below $0.2\,\mathrm{m\,s^{-1}}$ and above $0.2\,\mathrm{m\,s^{-1}}$, respectively (Fig. 7b). The results were similar to those of the BHOT, but the deviation of the MOST model results for the DOOT was smaller (Figs. 6a and 7a), and the fitted line for the DOOT was closer to the 1:1 scale line when the wave effects were considered (Figs. 6b and 7b). The observational heights of the eddy covariance systems were different between the BHOT (~17 m) and DOOT (~26 m) sites; however, the significant wave heights and wave spectra were approximately the same (Figs. 2b, 3b, and 4), which supported that the surface wave effects on the overlying wind field decreased as the observational height increased, as discussed by Hristov et al. (2003). Additionally, based on a wind-wave tank experiment Buckley and Veron (2018) showed that the wave influence on the

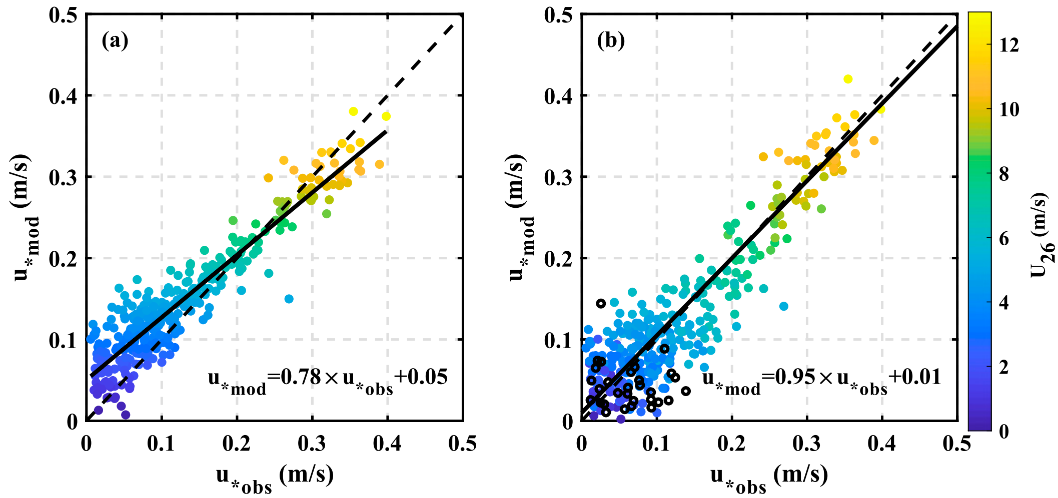

FIG. 7. As in Fig. 6, but for the DOOT observational periods.

airflow decreased with distance from the surface. Notably, the negative total stress was predicted by the S09 model using observed wave spectra under low wind conditions ($<4\,\mathrm{m\,s^{-1}}$, Figs. 6b and 7b), similar to the Donelan wave spectrum experimental results outlined in section 3a. The results again supported that the upward momentum flux existed under low-wind and swell-dominated conditions.

Based on comparisons between the modeled and observed wind stresses, the traditional MOST is not applicable to the air–sea interface where surface waves exist. Previous studies have concluded that the MOST is likely invalid over swell-dominated oceans (Drennan et al. 1999; Semedo et al. 2009; Högström et al. 2013; Jiang et al. 2016), which is supported by the results of our study. In addition, under higher wind speed and wind sea conditions, the MOST may not be suitable, which is in contrast to the suggestions of Smedman et al. (2003) and Drennan et al. (2003). Although Edson and Fairall (1998) suggested that the MOST is valid in marine conditions that are not influenced by wave-induced fluctuations, within the typical observational height ($<30\,\mathrm{m}$), the turbulent velocity was affected by the surface waves, which invalidated the MOST. Remarkably, Hanley and Belcher (2008) suggested that the swell can affect the whole marine atmospheric boundary layer (MABL), and Song et al. (2015) concluded that when considering the surface wave effects on the whole MABL, both swells and wind seas should be considered based on the model proposed by Hanley and Belcher(2008). Consequently, the MOST may be invalid throughout the MABL, however, further observations are needed beyond the use of simple models to illustrate this invalidity.

4. Conclusions

In this study, the impact of the ocean surface waves on the wind stress was qualitatively and quantitatively examined by comparing the constant flux model with field observations. Two turbulent eddy viscosities of the traditional MOST and a scheme including wave effects (Semedo et al. 2009) were used in the model, and the water depth factor was considered. Two observational sites with different water depths of 16 and 28 m in the coastal regions of the northern SCS and western ECS, respectively, were applied. The main results show that the ocean surface waves play a remarkable role in wind stress determination.

Under low-wind and strong-swell conditions, distinct peaks at the dominant swell frequency in the vertical velocity spectra were observed at different measurement heights. The swell-induced perturbation reached a height of nearly 30 m from the mean sea surface, which implied that the observed wind stress contained the wave-induced stress component, and this perturbation decreased with increasing height. Next, the influences of the fast-moving swell in finite-depth water on the wind profiles and the wind stress were evaluated by modeling the wave-induced stress. The wind profiles departed from the classical logarithmic profiles, and the deviation increased with the peak wave phase speed. Notably, the peak frequency of the wave spectra was fixed to the observed value of 0.115 Hz so that the deeper water induced a greater peak wave phase speed with more energy to impart to the wind, which produced a larger negative contribution to the wave-induced stress. The model also predicted an upward momentum transfer from the wave to the atmosphere at wind speeds below $4\,\mathrm{m\,s^{-1}}$, which was consistent with previous studies and observations; however, there are few observed cases.

Based on a comparison with the observations, the importance of surface waves in wind stress was confirmed. With respect to the traditional MOST, the model considering the wave effects (S09 model) better agreed with the observations. The fast swell would invalidate the traditional MOST, which was widely recognized; however, our results showed that the MOST may not be applicable even at higher wind speeds. Based on two different observational height results, the MOST was predicted to be invalid within the typical observational height (<30 m), and this invalidity decreased with height.

Only the observed along-wind or longitudinal stress was considered, and the surface wave direction was assumed to be along the wind direction in this study. Notably, the directions of the wind, wave, and stress are crucial factors that must be considered (Kudryavtsev and Makin 2004). Additionally, the wave growth/decay rate coefficient is the main source of uncertainty in the quantitative calculations of the model and significantly influences the model results; thus, additional theoretical and observational studies are needed to provide clear parameterization of this coefficient. Besides, the constant flux layer assumption used in this study may be debatable due to the stress divergence or the presence of horizontal pressure gradient (Mahrt et al. 2018), additional investigations are needed to analyze, such as three or more layers observations to determine.

Acknowledgment. This research was jointly supported by the National Key Research and Development Program of China Grants 2017YFC1404000 and 2016YFC1401403, and the corresponding author Fangli Qiao was also supported by the international cooperation project on the China-Australia Research Centre for Maritime Engineering of Ministry of Science and Technology, China under Grant 2016YFE0101400, and the NSFC-Shandong Joint Fund for Marine Science Research Centers under Grant U1606405. The authors are grateful to the platform maintenance personnel from the Guangzhou Institute of Tropical and Marine Meteorology and Wenzhou Marine Environmental Monitoring Center, and also appreciate that Dr. Zhongshui Zou from Zhejiang University provided his selfless help. The authors would like to thank the reviewers for their thoughtful comments and constructive suggestions that significantly helped us in improving our manuscript.

REFERENCES

Babanin, A. V., M. Onorato, and F. Qiao, 2012: Surface waves and wave-coupled effects in lower atmosphere and upper ocean. *J. Geophys. Res.*, **117**, C00J01, https://doi.org/10.1029/2012JC007932.

——, J. McConochie, and D. Chalikov, 2018: Winds near the surface of waves: Observations and modeling. *J. Phys. Oceanogr.*, **48**, 1079–1088, https://doi.org/10.1175/JPO-D-17-0009.1.

Belcher, S. E., and J. C. R. Hunt, 1993: Turbulent shear flow over slowly moving waves. *J. Fluid Mech.*, **251**, 109–148, https://doi.org/10.1017/S0022112093003350.

Buckley, M. P., and F. Veron, 2018: The turbulent airflow over wind generated surface waves. *Eur. J. Mech.*, **73B**, 132–143, https://doi.org/10.1016/j.euromechflu.2018.04.003.

Chen, S., F. Qiao, C. J. Huang, and B. Zhao, 2018: Deviation of wind stress from wind direction under low wind conditions. *J. Geophys. Res. Oceans*, **123**, 9357–9368, https://doi.org/10.1029/2018JC014137.

Cohen, J. E., and S. E. Belcher, 1999: Turbulent shear flow over fast-moving waves. *J. Fluid Mech.*, **386**, 345–371, https://doi.org/10.1017/S0022112099004383.

Donelan, M. A., J. Hamilton, and W. H. Hui, 1985: Directional spectra of wind-generated waves. *Philos. Trans. Roy. Soc. London*, **315A**, 509–562, https://doi.org/10.1098/rsta.1985.0054.

——, W. M. Drennan, and K. B. Katsaros, 1997: The air–sea momentum flux in conditions of wind sea and swell. *J. Phys. Oceanogr.*, **27**, 2087–2099, https://doi.org/10.1175/1520-0485(1997)027<2087:TASMFI>2.0.CO;2.

Drennan, W. M., K. K. Kahma, and M. A. Donelan, 1999: On momentum flux and velocity spectra over waves. *Bound.-Layer Meteor.*, **92**, 489–515, https://doi.org/10.1023/A:1002054820455.

——, H. C. Graber, D. Hauser, and C. Quentin, 2003: On the wave age dependence of wind stress over pure wind seas. *J. Geophys. Res.*, **108**, 8062, https://doi.org/10.1029/2000JC000715.

Edson, J. B., and C. W. Fairall, 1998: Similarity relationships in the marine atmospheric surface layer for terms in the TKE and scalar variance budgets. *J. Atmos. Sci.*, **55**, 2311–2328, https://doi.org/10.1175/1520-0469(1998)055<2311:SRITMA>2.0.CO;2.

Foken, T., R. Leuning, S. R. Oncley, M. Mauder, and M. Aubinet, 2012: Corrections and data quality control. *Eddy Covariance: A Practical Guide to Measurement and Data Analysis*, M. Aubinet, T. Vesala, and D. Papale, Eds., Springer, 85–131.

Grachev, A. A., and C. W. Fairall, 2001: Upward momentum transfer in the marine boundary layer. *J. Phys. Oceanogr.*, **31**, 1698–1711, https://doi.org/10.1175/1520-0485(2001)031<1698:UMTITM>2.0.CO;2.

——, ——, J. E. Hare, J. B. Edson, and S. D. Miller, 2003: Wind stress vector over ocean waves. *J. Phys. Oceanogr.*, **33**, 2408–2429, https://doi.org/10.1175/1520-0485(2003)033<2408:WSVOOW>2.0.CO;2.

Grare, L., L. Lenain, and W. K. Melville, 2013: Wave-coherent airflow and critical layers over ocean waves. *J. Phys. Oceanogr.*, **43**, 2156–2172, https://doi.org/10.1175/JPO-D-13-056.1.

Hanley, K. E., and S. E. Belcher, 2008: Wave-driven wind jets in the marine atmospheric boundary layer. *J. Atmos. Sci.*, **65**, 2646–2660, https://doi.org/10.1175/2007JAS2562.1.

Hare, J. E., T. Hara, J. B. Edson, and J. M. Wilczak, 1997: A similarity analysis of the structure of airflow over surface waves. *J. Phys. Oceanogr.*, **27**, 1018–1037, https://doi.org/10.1175/1520-0485(1997)027<1018:ASAOTS>2.0.CO;2.

Högström, U., A. Rutgersson, E. Sahlée, A. S. Smedman, T. S. Hristov, W. M. Drennan, and K. K. Kahma, 2013: Air-sea interaction features in the Baltic Sea and at a Pacific trade-wind site: An inter-comparison study. *Bound.-Layer Meteor.*, **147**, 139–163, https://doi.org/10.1007/s10546-012-9776-8.

——, E. Sahlée, A. S. Smedman, A. Rutgersson, E. Nilsson, K. K. Kahma, and W. M. Drennan, 2015: Surface stress over the ocean in swell-dominated conditions during moderate winds. *J. Atmos. Sci.*, **72**, 4777–4795, https://doi.org/10.1175/JAS-D-15-0139.1.

Hristov, T. S., C. A. Friehe, and S. D. Miller, 1998: Wave-coherent fields in air flow over ocean waves: Identification of cooperative behavior buried in turbulence. *Phys. Rev. Lett.*, **81**, 5245–5248, https://doi.org/10.1103/PhysRevLett.81.5245.

——, S. D. Miller, and C. A. Friehe, 2003: Dynamical coupling of wind and ocean waves through wave-induced air flow. *Nature*, **422**, 55–58, https://doi.org/10.1038/nature01382.

Huang, N. E., S. R. Long, P. A. Hwang, H. Wang, and L. F. Bliven, 1983: A study on the spectral models for waves in finite water depth. *J. Geophys. Res.*, **88**, 9579–9587, https://doi.org/10.1029/JC088iC14p09579.

Janssen, P. A. E. M., 1989: Wave-induced stress and the drag of air flow over sea waves. *J. Phys. Oceanogr.*, **19**, 745–772, https://doi.org/10.1175/1520-0485(1989)019<0745:WISATD>2.0.CO;2.

——, 1992: Experimental evidence of the effect of surface waves on the airflow. *J. Phys. Oceanogr.*, **22**, 1600–1604, https://doi.org/10.1175/1520-0485(1992)022<1600:EEOTEO>2.0.CO;2.

Jiang, Q., P. Sullivan, S. Wang, J. Doyle, and L. Vincent, 2016: Impact of swell on air–sea momentum flux and marine boundary layer under low-wind conditions. *J. Atmos. Sci.*, **73**, 2683–2697, https://doi.org/10.1175/JAS-D-15-0200.1.

Komen, G. I., 1994: Wave growth by wind. *Dynamics and Modelling of Ocean Waves*, G. I. Komen et al., Eds., Cambridge University Press, 102–112.

Kudryavtsev, V. N., and V. K. Makin, 2004: Impact of swell on the marine atmospheric boundary layer. *J. Phys. Oceanogr.*, **34**, 934–949, https://doi.org/10.1175/1520-0485(2004)034<0934:IOSOTM>2.0.CO;2.

Mahrt, L., S. Miller, T. Hristov, and J. Edson, 2018: On estimating the surface wind stress over the sea. *J. Phys. Oceanogr.*, **48**, 1533–1541, https://doi.org/10.1175/JPO-D-17-0267.1.

Makin, V. K., 2008: On the possible impact of a following-swell on the atmospheric boundary layer. *Bound.-Layer Meteor.*, **129**, 469–478, https://doi.org/10.1007/s10546-008-9320-z.

——, H. Branger, W. L. Peirson, and J. P. Giovanangeli, 2007: Stress above wind-plus-paddle waves: Modeling of a laboratory experiment. *J. Phys. Oceanogr.*, **37**, 2824–2837, https://doi.org/10.1175/2007JPO3550.1.

Nilsson, E. O., A. Rutgersson, A. S. Smedman, and P. P. Sullivan, 2012: Convective boundary-layer structure in the presence of wind-following swell. *Quart. J. Roy. Meteor. Soc.*, **138**, 1476–1489, https://doi.org/10.1002/qj.1898.

Plant, W. J., 1982: A relationship between wind stress and wave slope. *J. Geophys. Res.*, **87**, 1961–1967, https://doi.org/10.1029/JC087iC03p01961.

Rieder, K. F., and J. A. Smith, 1998: Removing wave effects from the wind stress vector. *J. Geophys. Res.*, **103**, 1363–1374, https://doi.org/10.1029/97JC02571.

Semedo, A., Ø. Saetra, A. Rutgersson, K. K. Kahma, and H. Pettersson, 2009: Wave-induced wind in the marine boundary layer. *J. Atmos. Sci.*, **66**, 2256–2271, https://doi.org/10.1175/2009JAS3018.1.

Smedman, A., U. Högström, H. Bergström, A. Rutgersson, K. K. Kahma, and H. Pettersson, 1999: A case study of air-sea interaction during swell conditions. *J. Geophys. Res.*, **104**, 25 833–25 851, https://doi.org/10.1029/1999JC900213.

——, X. Guo Larsén, U. Högström, K. K. Kahma, and H. Pettersson, 2003: Effect of sea state on the momentum exchange over the sea during neutral conditions. *J. Geophys. Res.*, **108**, 3367, https://doi.org/10.1029/2002JC001526.

——, U. Högström, E. Sahlée, W. M. Drennan, K. K. Kaham, and H. Pettersson, 2009: Observational study of marine atmospheric boundary layer characteristics during swell. *J. Atmos. Sci.*, **66**, 2747–2763, https://doi.org/10.1175/2009JAS2952.1.

Song, J., W. Fan, S. Li, and M. Zhou, 2015: Impact of surface waves on the steady near-surface wind profiles over the ocean. *Bound.-Layer Meteor.*, **155**, 111–127, https://doi.org/10.1007/s10546-014-9983-6.

Uz, B. M., T. Hara, E. J. Bock, and M. A. Donelan, 2003: Laboratory observations of gravity-capillary waves under transient wind forcing. *J. Geophys. Res.*, **108**, 3050, https://doi.org/10.1029/2000JC000643.

Veron, F., W. K. Melville, and L. Lenain, 2009: Measurements of ocean surface turbulence and wave-turbulence interactions. *J. Phys. Oceanogr.*, **39**, 2310–2323, https://doi.org/10.1175/2009JPO4019.1.

Zhao, Z. K., C. X. Liu, Q. Li, G. F. Dai, Q. T. Song, and W. H. Lv, 2015: Typhoon air-sea drag coefficient in coastal regions. *J. Geophys. Res. Oceans*, **120**, 716–727, https://doi.org/10.1002/2014JC010283.

Zou, Z., D. Zhao, J. Zhang, S. Li, Y. Cheng, H. Lv, and X. Ma, 2018: The influence of swell on the atmospheric boundary layer under nonneutral conditions. *J. Phys. Oceanogr.*, **48**, 925–936, https://doi.org/10.1175/JPO-D-17-0195.1.